An Insight Into the Internal Consistency of MODIS Global Leaf Area Index Products

Xingjian Zhang, Kai Yan, Jinxiu Liu, Kai Yang, Jiabin Pu, Guangjian Yan, *Senior Member, IEEE*, Janne Heiskanen, Peng Zhu, Yuri Knyazikhin, and Ranga B. Myneni

***Abstract*— The evaluation and validation of climate data records (CDRs) derived from remote sensing play crucial roles in their generation and applications. However, many existing evaluation schemes rely on simplistic, spatiotemporally invariant metrics to assess the products' overall quality, which leads to the long-term neglect of intra-product inconsistencies stemming from observation conditions, algorithmic differences, and sensor degradation. Leaf area index (LAI) is a crucial variable for land surface and climate modeling, and the intra-product inconsistency will increase the uncertainty in related studies. In order to improve the evaluation scheme of LAI products and ensure their reliability, we propose a new perspective for evaluating global LAI time series. In this study, we utilize the Moderate Resolution Imaging Spectroradiometer (MODIS) C6.1 LAI product as an example to infer its internal consistency through cross-comparisons among different sensors and spatiotemporal correlations between two adjacent years of the product. We found that compared to the main algorithm, the backup algorithm of the MODIS LAI product tends to underestimate the retrieval results. This inconsistency is particularly pronounced in tropical regions but relatively minor in most other areas. Additionally, these inconsistencies can lead to unusual fluctuations in the LAI time series, impacting the magnitude and direction of short-term vegetation monitoring. However, the influence on long-term trend analyses is negligible. Therefore, special attention should be given to the intra-product consistency in certain studies. In conclusion, the evaluation perspective proposed in this study is of great significance for improving the LAI evaluation scheme and ensuring the use and improvement of remote sensing products.**

***Index Terms*— Climate data record (CDR), internal consistency, leaf area index (LAI), Moderate Resolution Imaging Spectroradiometer (MODIS), product evaluation.**

Manuscript received 28 April 2024; revised 24 June 2024; accepted 21 July 2024. Date of publication 29 July 2024; date of current version 12 August 2024. This work was supported in part by the National Natural Science Foundation of China under Grant 42192580 and Grant 42271356. *(Corresponding author: Kai Yan.)*

Xingjian Zhang, Kai Yan, and Guangjian Yan are with the Innovation Research Center of Satellite Application (IRCSA), State Key Laboratory of Remote Sensing Science, Faculty of Geographical Science, Beijing Normal University, Beijing 100875, China (e-mail: xingjianzhang@email.cugb.edu.cn; kaiyan@bnu.edu.cn; gjyan@bnu.edu.cn).

Jinxiu Liu and Kai Yang are with the School of Information Engineering and the School of Land Science and Techniques, China University of Geosciences, Beijing 100083, China (e-mail: jinxiuliu@cugb.edu.cn; kaiyang@email.cugb.edu.cn).

Jiabin Pu, Yuri Knyazikhin, and Ranga B. Myneni are with the Department of Earth and Environment, Boston University, Boston, MA 02215 USA (e-mail: om7759@bu.edu; jknjazi@bu.edu; ranga.myneni@gmail.com).

Janne Heiskanen is with the Department of Geosciences and Geography, University of Helsinki, 00014 Helsinki, Finland, and also with the Finnish Meteorological Institute, 00101 Helsinki, Finland (e-mail: janne.heiskanen@helsinki.fi).

Peng Zhu is with the Department of Geography and the Institute for Climate and Carbon Neutrality, University of Hong Kong, Hong Kong SAR, China (e-mail: zhupeng@hku.hk).

Digital Object Identifier 10.1109/TGRS.2024.3434366

I. Introduction

CLIMATE data records (CDRs) are time series of measurements that have sufficient length, consistency, and continuity. They offer reliable insights into the occurrence, extent, and spatial distribution of changes in land, oceans, atmosphere, and ice sheets, thereby aiding in the assessment of climate variability and change [1]. As an essential climate variable (ECV) recognized by the Global Climate Observing System (GCOS), leaf area index (LAI) is a pivotal component of CDRs [2]. LAI is commonly defined as half of the total green leaf area per unit of horizontal ground area [3], [4], serving to characterize the structure and function of vegetation canopies [5]. Moreover, LAI serves as a critical parameter in global carbon cycle, climate, hydrology, biogeochemistry, and ecology models [6], [7], [8]. It also acts as a fundamental input for various land surface process models [9], [10], [11], [12] and plays a crucial role in studies related to vegetation productivity and water use efficiency [3].

To ensure the reliability and accuracy of studies concerning global climate change, climate impacts, the carbon cycle, and emission source estimation, GCOS has established standards for satellite-derived datasets and products. These standards encompass various aspects, including spatial and temporal resolution, accuracy, and stability [2]. Based on these standards, extensive evaluation and validation efforts have been conducted to assess the quality and reliability of satellite-derived CDR data. Regarding LAI products, these efforts primarily involve direct comparisons with ground measurements [13], [14], [15], comparisons with upscaled high-resolution reference datasets [16], [17], [18], cross-validation among various LAI products or their iterative releases [19], [20], [21], [22], and comparisons with model-simulated LAI [23], [24], [25]. Factors such as cloud contamination, large-angle observations, and ice/snow cover can introduce variations in the accuracy of reflectance products across different time and geographical locations. Consequently, LAI products often employ different retrieval algorithms tailored to varying observation qualities. However, these studies often neglect internal inconsistencies in the inversion algorithms caused by factors such as observation quality, which can lead to differences in the precision, accuracy, stability, and physical significance of the inversion results [19], [20], [21], [26].

Moderate Resolution Imaging Spectroradiometer (MODIS) LAI products are well-known for their clear physical interpretation, high spatial and temporal resolution, free accessibility,

TABLE I
SEVERAL GLOBAL MODERATE RESOLUTION LAI PRODUCTS

Products	Sensor	Version	Spatial resolution	Temporal resolution	Algorithm paths or quality flags	References
PROBA-V	PROBA-V	V1	300 m	10-day (2014−)	1. EBF case: 1) based on daily observations; 2) based on previous dekadal product 2. Non-EBF case: 1) second degree polynomials fit; 2) linear fit; 3) interpolation between the two nearest dates	[27]
EUMETSAT Polar System	MetOp / AVHRR	V1	1.1 km	10-day (2015−)	1. Ice / Atmospheric Anomaly Indicator (σ_{GPR}) 2. BRDF reliability indicator (σ_{k_0}) 3. Overall error indicator (Err (LAI))	[28]
GEOV2	SPOT / VEGETATION, MODIS	V2	1 / 112°	10-day (1999−)	1. Direct retrieval 2. Climatology-based retrieval 3. Interpolation-based retrieval	[29]
MODIS	Terra / Aqua	C6	500 m	8-day (2000−)	1. Main algorithm based on radiative transfer model 2. Backup algorithm based on LAI-NDVI empirical relationship	[19, 20]
GLASS	MODIS	V6	250 m / 500m	8-day (2000−)	1. Solar zenith angle less than 85°: Predict using the Bi-LSTM model 2. Solar zenith angle greater than 85°: Interpolate using the nearby days' valid LAI values	[30]
VIIRS	SNPP / VIIRS	V1	500 m	8-day (2012−)	1. Main algorithm based on radiative transfer model 2. Backup algorithm based on LAI-NDVI empirical relationship	[31]

and global coverage [32]. The MODIS LAI product uses a main algorithm based on a 3-D radiative transfer (3-D RT) equation and a backup algorithm based on the empirical relationship between the normalized difference vegetation index (NDVI) and LAI/FPAR [19]. The backup algorithm is activated only when the uncertainty of the input surface reflectance product is high enough to cause the main algorithm to fail. Similar to the MODIS LAI product, several commonly used LAI products contain results derived from different algorithms or varying qualities (see Table I). The PROBA-V LAI product employs a specialized processing technique for broadleaf evergreen forests. This is necessary because these forests are highly influenced by cloud cover, resulting in increased noise levels (false cloud detection) and missing data. Furthermore, three distinct computational methods were utilized to temporally smooth and synthesize instantaneous LAI estimates for other vegetation types [27]. The EUMETSAT Polar System (EPS) LAI product provides three quality indicators: σ_{GPR}, σ_{k_0}, and Err (LAI). These indicators help identify invalid outliers, assess the reliability of the bidirectional reflectance distribution function (BRDF), and estimate overall errors. The uncertainty value determines the quality classification of EPS LAI products into three categories: good, medium, and poor [28]. In addition, influenced by factors such as the observation quality or the amount of valid data, there are three retrieval methods for the GEOV2 LAI product: direct retrieval, climatology-based retrieval, and interpolation-based retrieval [21], [29]. The GLASS V6 LAI product generates the LAI product from the MODIS reflectance data using bidirectional long-short term memory (Bi-LSTM). However, the Bi-LSTM model can only predict valid LAI values when the atmospherically corrected surface reflectance is above 70°N and the solar zenith angle (SZA) is less than 85°. Pixels with SZA greater than 85° can only be obtained by interpolating from nearby days [30]. As a continuation of MODIS LAI products, the VIIRS LAI product also comprises different algorithm paths [31]. These products exhibit clear internal inconsistencies, yet systematic internal consistency evaluations are lacking.

Internal inconsistencies in the satellite-derived LAI product increase the uncertainty in the overall product. These uncertainties ultimately lead to uncertainties in downstream applications. Therefore, there is an urgent need to quantitatively and qualitatively evaluate the internal consistency of global LAI products, which is crucial for improving the modeling of land surface and climate, as well as accurately monitoring global vegetation. In this study, we use the MODIS C6.1 LAI product as an example to introduce a new perspective for validating and evaluating remote sensing data products. Specifically, it emphasizes that intra-product results should have consistent performance and behavior under similar spatial and temporal conditions. The research will help improve

the framework for validating and assessing remote sensing data products, as well as offer guidance for their use and refinement.

This article is organized as follows. Sections II and III describe the dataset and methodology used to assess the internal consistency. In Section IV, we compare the spatiotemporal distribution of the retrieval results from different algorithms, the internal consistency of the MODIS LAI product, and the impact of internal inconsistency on long-time series trend tests. Section V discusses the causes of internal inconsistencies, potential impacts on product applications, and directions for improvement in detail. Finally, Section VI provides concluding remarks.

II. Datasets

A. MODIS C6.1 LAI Products

The latest version of the MODIS LAI product is Collection 6.1 (MODIS C6.1 LAI products), which was publicly released in April 2020. It includes LAI products from Terra MODIS, Aqua MODIS, and the Terra + Aqua MODIS combination [33]. Terra's LAI products (MOD15A2H) cover the period from 2000 to the present, while Aqua's products (MYD15A2H) cover the period from 2002 to the present. No changes have been made to the scientific algorithms for the MODIS C6.1 LAI products. Any improvements or differences compared to the previous C6 version are the result of improved calibration methods for the MODIS L1B products, as well as updates to the polarization corrections applied during the reprocessing [33]. In this study, we used the MODIS C6.1 LAI products (MOD15A2H, MYD15A2H) for our analyses, which have a standard data product with a spatial resolution of 500 m and a temporal resolution of 8 days. It typically produces 46 composites per year, but one or two composites may be lost due to sensor problems or other factors. All MODIS LAI products are available via LP DAAC (https://lpdaac.usgs.gov/products/mod15a2hv061/).

The MODIS LAI operational algorithm is composed of a main algorithm and a backup algorithm. The main algorithm is based on the radiative transfer equation (RTE), while the backup algorithm relies on the empirical correlation between the NDVI and canopy LAI. The input data includes bidirectional reflectance factors (BRFs) in the red and near-infrared bands, their uncertainties, four observation geometries, and a biome classification map [33]. According to the quality control document, the main algorithm can be categorized as "Main algorithm without saturation" (QA = 0) and "Main algorithm with saturation" (Main-S) (QA = 1). Backup algorithms can be categorized into "BackUp-G algorithm" (QA = 2), which is caused by poor observation geometry and "BackUp-O algorithm" (QA = 3), which is caused by problems other than geometry. The algorithm path information is stored in the "FparLai_QC" layer for user reference.

B. MODIS Land Cover Product

The MCD12Q1 dataset is a MODIS land cover product that provides an annual global distribution of land cover types at a 500-m resolution. It is derived from supervised classification of MODIS reflectance data and is further refined through post-processing and integration of auxiliary information to optimize specific categories [34]. In this study, the LAI product's internal consistency was analyzed using a classification scheme based on the LAI/FPAR classification of vegetation (LC_Type3). For this scheme, global vegetation is categorized into eight biomes. The eight biomes are (B1) grasses and cereal crops, (B2) shrubs, (B3) broadleaf crops, (B4) savannas, (B5) evergreen broadleaf forest (EBF), (B6) deciduous broadleaf forest (DBF), (B7) evergreen needleleaf forest (ENF), and (B8) deciduous needleleaf forest (DNF). The MCD12Q1 C6.1 product is available via LP DAAC (https://lpdaac.usgs.gov/products/mcd12q1v061/).

III. Methodology

A. Framework for Evaluating Internal Consistency

An evaluation framework has been devised to assess the internal consistency of the MODIS C6.1 LAI product, as illustrated in Fig. 1. The framework comprises an evaluation of intra-product consistency and an analysis of its impact on vegetation monitoring. In this study, we initially pre-processed the land cover and LAI products. Subsequently, we inferred internal consistency through cross-comparisons between the various algorithm retrieval results of Terra and Aqua products and spatiotemporal correlation analysis of the Terra LAI product over two adjacent years. Finally, to investigate the impact of internal inconsistency on long-term trend analyses, we compared the consistency of LAI trends across different algorithmic control methods. This framework is an important reference for evaluating the internal consistency of CDR products with multiple algorithmic branches.

B. Data Pre-Processing

In this study, we first reduced the spatial resolution of the LAI products and MCD12Q1 to 5 × 5 km using the nearest neighbor sampling method. This approach allowed us to reduce the data volume and enhance computational efficiency. Subsequently, we masked the non-vegetated areas (water bodies, bare land, urban, permanent snow, and ice) in each year's LAI product using each year's MCD12Q1 product to minimize the impact on the study results. Finally, we extracted the main algorithm LAI (QA = 0 and QA = 1) and the backup algorithm LAI (QA = 2 and QA = 3) based on the "FparLai_QC" layer for further analysis.

C. Inferring Product Internal Consistency Through Terra and Aqua Product Cross-Comparisons

The Terra MODIS LAI (MOD15A2H) and Aqua MODIS LAI (MYD15A2H) products demonstrate a high degree of consistency and comparability, owing to the employment of identical sensor types, inversion algorithms, and multiday synthesis methods [35]. Therefore, the internal consistency of MODIS LAI products can be inferred by comparing the differences in different algorithm LAI of the two sensors. The differences include the main algorithm LAI (Both Main), backup algorithm LAI (Both BackUp), MOD15A2H's

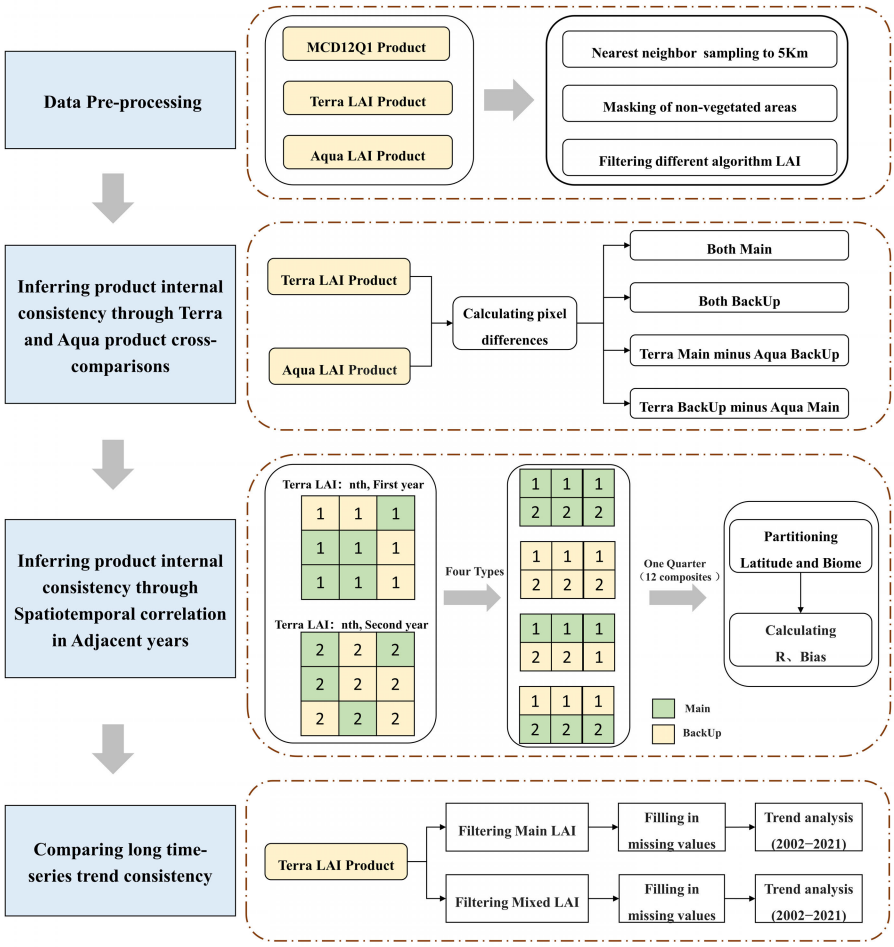

Fig. 1. Framework of internal consistency evaluation.

main algorithm LAI and MYD15A2H's backup algorithm LAI (MOD Main–MYD BackUp), and MYD15A2H's main algorithm LAI and MOD15A2H's backup algorithm LAI (MOD BackUp–MYD Main). If the differences between the different algorithm LAI are similar to the "Both Main" scenario, this indicates good consistency in the MODIS LAI product. To minimize the effect of individual extremes or outliers and to improve reliability and stability, we calculated a multiyear average of the LAI difference for each composite data, the equations are as follows:

$$\delta \mathrm{LAI}_t = \mathrm{LAI}_{\mathrm{MOD}(i)} - \mathrm{LAI}_{\mathrm{MYD}(j)} \tag{1}$$

$$\delta \mathrm{LAI}_s = \frac{\sum_{t=n}^{n+11} \delta \mathrm{LAI}_t}{12} \quad (s = \mathrm{MAM, JJA, SON, DJF}) \tag{2}$$

$$\delta \mathrm{LAI} = \frac{\sum_{y=2003}^{y+19} (\delta \mathrm{LAIs})_y}{19} \tag{3}$$

where $\delta \mathrm{LAI}_t$ represents the difference between the tth composite of the two products, i, j represents the algorithm path, $\delta \mathrm{LAI}_s$ represents the mean difference between the 12 composites in a quarter, n represents the number of initial composites of the quarter s, and δLAI denotes the mean of $\delta \mathrm{LAI}_s$ for a total of 19 years between 2003 and 2021. MAM: March–April–May; JJA: June–July–August; SON: September–October–November; DJF: December–January–February.

D. Inferring Product Internal Consistency Through Spatiotemporal Correlation of Adjacent Years

According to the first law of geography, everything is connected, but objects that are in close proximity are typically more closely connected to each other than those that are farther apart [36]. Vegetation in adjacent years can be influenced by various factors, including inter-annual meteorological changes, natural growth and decline, and human activities. However, a strong correlation is generally anticipated among pixel pairs located at the same location and season on a global scale. The LAI products with higher quality, greater inversion accuracy, and increased algorithmic robustness and stability are better able to capture this correlation. By analyzing the spatiotemporal correlations between different LAI algorithms over two adjacent years, we can assess intra-product consistency and evaluate the impact of algorithmic changes on short-term vegetation monitoring.

To comprehensively compare the consistency of algorithms, we initially matched LAI pixels for the same composite period in two adjacent years one by one. Subsequently, we categorized the global two-year pixel pairs according to latitudinal bands, seasons, and biome types. Finally, we computed the correlation coefficients (R) and mean bias (Bias) of the pixel pairs for the neighboring years, with R and Bias determined

using the following equations:

$$R = \frac{\sum_{i=1}^{n}(x_i - \bar{x})(y_i - \bar{y})}{\sqrt{\sum_{i=1}^{n}(x_i - \bar{x})^2 \sum_{i=1}^{n}(y_i - \bar{y})^2}} \tag{4}$$

$$\text{Bias} = \frac{\sum_{i=1}^{n}(y_i - x_i)}{n} \tag{5}$$

where x_i and y_i denote the ith individual LAI value in the set of pixel pairs, $\bar{x}$ and $\bar{y}$ represent the mean LAI values of the pixel sets in the first and second year, respectively.

The algorithm changes for pixels over the two years can be categorized into four groups: Both Main (using the main algorithm in both years), Both Backup (using the backup algorithm in both years), Main to Backup (changing from the main algorithm to the backup algorithm), and Backup to Main (changing from the backup algorithm to the main algorithm). To enhance study reliability, we calculated the mean values of R and Bias for the periods 2003–2004, 2010–2011, and 2020–2021 for analysis. If the R and Bias in the "Both Main" scenario are similar to the other three algorithm scenarios, it indicates that there is consistency in the inversion results of the different algorithms. This also suggests that changes in algorithmic paths have a minimal impact on short-term vegetation monitoring.

E. Comparing Long Time-Series Trend Consistency

In order to analyze the effect of internal inconsistencies on the trend analysis of LAI long time series, we compared the trends of the main algorithm LAI (Main LAI) and the LAI of the mixed all algorithms (Mixed LAI). For missing values in the two sets of time-series data, we used the simple arithmetic mean method in climatology to fill them in. This method calculates multiyear averages contemporaneous with the missing values as the filled data [37]. In order to avoid time-series data being mostly filled data, we masked pixels with less than one-third of the effective data volume over the 20 years. In this study, the data used for filling are the 20-year averages from 2002 to 2021. We used the northern hemisphere growing season average LAI (GSA LAI) for the analysis. Referring to previous studies [38], [39], we defined the vegetation growing season in the northern hemisphere as May to September each year. This period is the peak and critical period of vegetation growth. The GSA LAI can be given based on the following:

$$\text{GSA LAI} = \frac{\sum_{i=1}^{16}\text{LAI}_i}{16} \tag{6}$$

where GSA LAI represents the average LAI of 16 composites for a given pixel over the growing season.

The coefficient of variation (CV) was utilized to measure the fluctuation in the GSA LAI over the time series. This metric provides a dimensionless measure that is independent of the unit and absolute value of the variable [40], [41]. A higher CV value indicates a greater annual variation in GSA LAI, while a lower CV value indicates a more stable GSA LAI. The CV can be calculated as

$$\text{CV} = \frac{\text{Std}(X)}{\text{Mean}(X)} \tag{7}$$

where $\text{Std}(X)$ and $\text{Mean}(X)$ represent the standard deviation and mean of the GSA LAI from 2002 to 2021, respectively.

The Mann–Kendal (MK) test is a trend analysis tool recommended by the World Meteorological Organization (WMO) [42]. It was first proposed by Mann [44] and reformulated by Kendall [43]. In this study, the MK test was used to analyze the trend of multiyear GSA LAI. The MK test statistic (S) can be expressed by

$$S = \sum_{i=1}^{n-1}\sum_{j=i+1}^{n}\text{sgn}(x_j - x_i) \tag{8}$$

where x_i and x_j represent data points in the time series and satisfy the following:

$$\text{sgn}(x_j - x_i) = \begin{cases} +1, & (x_j - x_i) > 0 \\ 0, & (x_j - x_i) = 0 \\ -1, & (x_j - x_i) < 0. \end{cases} \tag{9}$$

The variance estimate for S is given by the following:

$$\text{var}(S_t) = \frac{n(n-1)(2n+5) - \sum_{i=1}^{m} t_i(t_i-1)(2t_i+5)}{18} \tag{10}$$

where m represents the number of tied groups, and t_i represents the size of the ath value within tied groups. The MK statistic (Z) can be obtained using the following:

$$Z = \begin{cases} \dfrac{S_t - 1}{\sqrt{\text{var}(S_t)}}, & S_t > 0 \\ 0, & S_t = 0 \\ \dfrac{S_t + 1}{\sqrt{\text{var}(S_t)}}, & S_t < 0. \end{cases} \tag{11}$$

The null hypothesis (i.e., no trend) is rejected when $|Z| > Z1\text{–}\alpha/2$, where α is the specific significance level. When $|Z|$ is greater than or equal to 1.64 ($\alpha = 0.1$), 1.96 ($\alpha = 0.05$), and 2.58 ($\alpha = 0.01$), the time series passes the significance test at the 90%, 95%, and 99% confidence levels, respectively. In this article, $\alpha = 0.1$ has been chosen in order to obtain as many comparisons as possible.

In this study, the magnitude of the trend is assessed using Sen's estimator of the slope [45], and calculated as follows:

$$S_i = \frac{x_b - x_a}{b - a}, \quad i = 1, \ldots, N \tag{12}$$

where x_a and x_b represent the time-series values at time points a and b, respectively (where $b > a$). The median of the N values for S_i was taken to obtain the Sen's slope estimator. A positive value of Sen's slope estimator indicates an upward trend, while a negative value indicates a downward trend.

IV. Results

A. Spatiotemporal Distribution of Algorithm Paths

Fig. 2 illustrates the global distribution of the backup algorithm inversion rate across the various seasons of the global MOD15A2H in 2021. The regions with a high rate of backup algorithms are concentrated in high-latitude regions of the northern hemisphere and tropical regions. During winter (DJF), the backup algorithms exhibit a higher rate, particularly in the high-latitude regions of the northern hemisphere, where

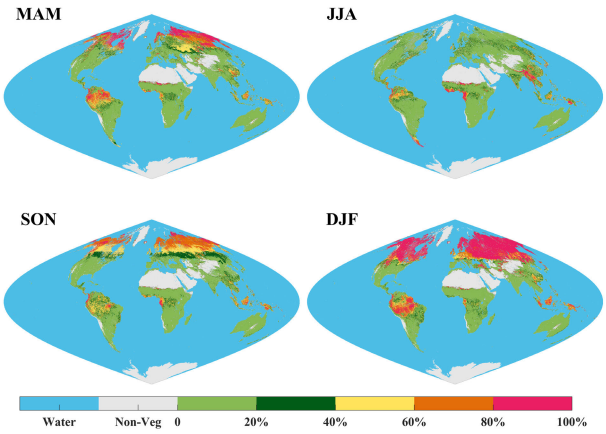

Fig. 2. Global distribution of the rate of pixel-by-pixel backup algorithms for four periods in 2021. MAM: March–April–May; JJA: June–July–August; SON: September–October–November; DJF: December–January–February.

the rate exceeds 80% in most areas. Conversely, a lower rate is observed during summer (JJA). Regarding vegetation types, the rate of backup algorithms is lower in summer compared to winter, particularly in biome types 7 and 8 (see Fig. 3). This difference can be attributed to the lower SZA in winter at high latitudes, which leads to the failure of the main algorithm and the activation of the backup algorithm. Notably, biome types 7 and 8 are primarily distributed in the high-latitude regions of the northern hemisphere.

Fig. 4 presents frequency distribution and box plots of monthly average LAI for the main and backup algorithms. The analysis was limited to pixels with both the main and backup algorithm LAI in a given month. The main and backup algorithms exhibited similar numerical distributions for grasses/cereal crops and broadleaf crops (except JJA). However, for other biome types, the backup algorithm's LAI box plots indicated relatively lower median, upper quartile, and lower quartile values, particularly in EBFs. This suggests that there are more backup algorithm pixels with LAI values predominantly distributed in the lower range.

B. Cross-Comparison of Terra/Aqua Products

Fig. 5 illustrates the global spatial distribution pattern of LAI differences between different algorithm paths for the Terra and Aqua LAI products. When the algorithms were consistent, the differences between the two sensors were minimal. However, when the algorithms differed, the differences became more pronounced, with the backup algorithm LAI underestimating the main algorithm. The absolute value of the global mean difference when comparing the same algorithms ("Both Main" and "Both Backup") was below 0.08 for all seasons. However, the "MOD Main–MYD Backup" and "MOD Backup–MYD Main" values exceeded 0.15. Specifically, the "MOD Main–MYD Backup" value was positive, while "MOD Backup–MYD Main" was negative. In most latitude zones, the difference is small when the algorithm paths of the two sensors are the same, but larger when the algorithm paths are different (see Fig. 6). In the tropical zone, the difference between the backup algorithm and the main algorithm reaches a maximum

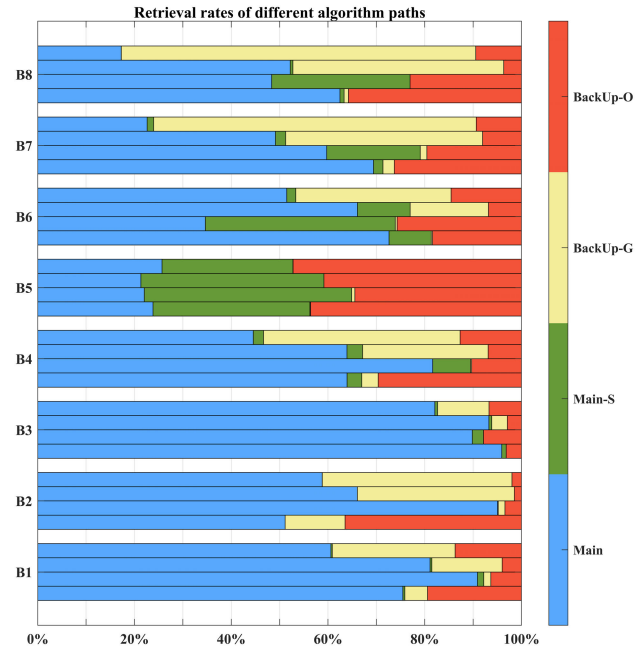

Fig. 3. Retrieval rates of different algorithm paths for different biome types globally. Comparisons are made for the four periods: MAM, JJA, SON, and DJF (four bars from bottom to top).

TABLE II
PERCENTAGE OF LAI DIFFERENCES BETWEEN DIFFERENT ALGORITHMS FOR TERRA AND AQUA

Algorithm differences	Seasons	Within ±0.5	[±0.5, ±1.5]	Over ±1.5
Both Main	MAM	95.69%	3.80%	0.51%
	JJA	95.36%	4.27%	0.37%
	SON	93.62%	5.96%	0.42%
	DJF	95.73%	3.82%	0.45%
Both BackUp	MAM	87.41%	10.87%	1.72%
	JJA	81.36%	16.26%	2.38%
	SON	88.72%	9.94%	1.34%
	DJF	88.67%	10.01%	1.33%
MOD Main – MYD BackUp	MAM	80.28%	16.25%	3.47%
	JJA	76.14%	20.46%	3.40%
	SON	80.40%	16.08%	3.52%
	DJF	80.84%	15.56%	3.61%
MOD BackUp – MYD Main	MAM	79.74%	14.61%	5.65%
	JJA	77.55%	18.62%	3.83%
	SON	82.21%	15.88%	1.92%
	DJF	77.59%	16.98%	5.42%

and shows an underestimation. This may be due to the fact that when the vegetation is denser, NDVI does not provide more information about the vegetation due to the saturation effect.

The percentage of LAI differences for the different algorithms for the two sensors is shown in Table II. In the "Both Main" scenario, more than 85% of the retrievals

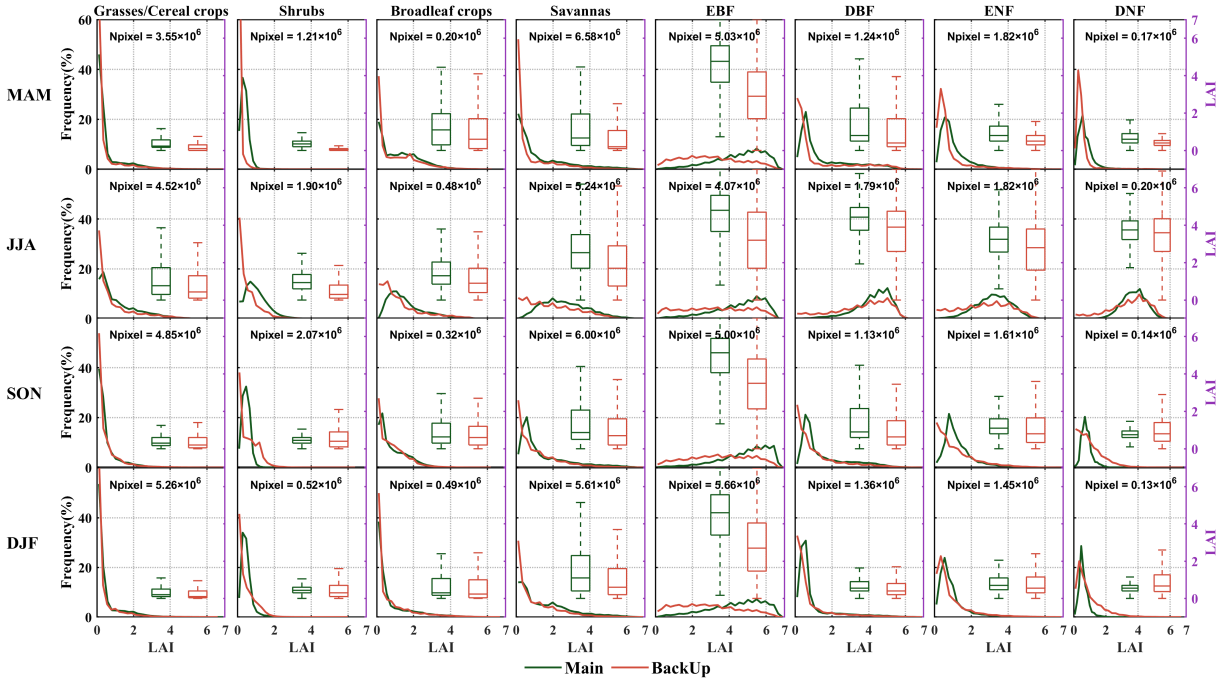

Fig. 4. Histogram and box plots of monthly average LAI for the main and backup algorithms for the period 2017–2021, including median, quartiles, and whiskers. Only pixels with both main and backup algorithms in one month were used as analysis pixels. Bin in the frequency distribution histogram is 30. The first y-axis (left) represents the y-axis of the histogram of the frequency distribution and the second y-axis (right) represents the y-axis of the box plots. Only pixels with no change in land cover between 2017 and 2021 were used as analyzed pixels.

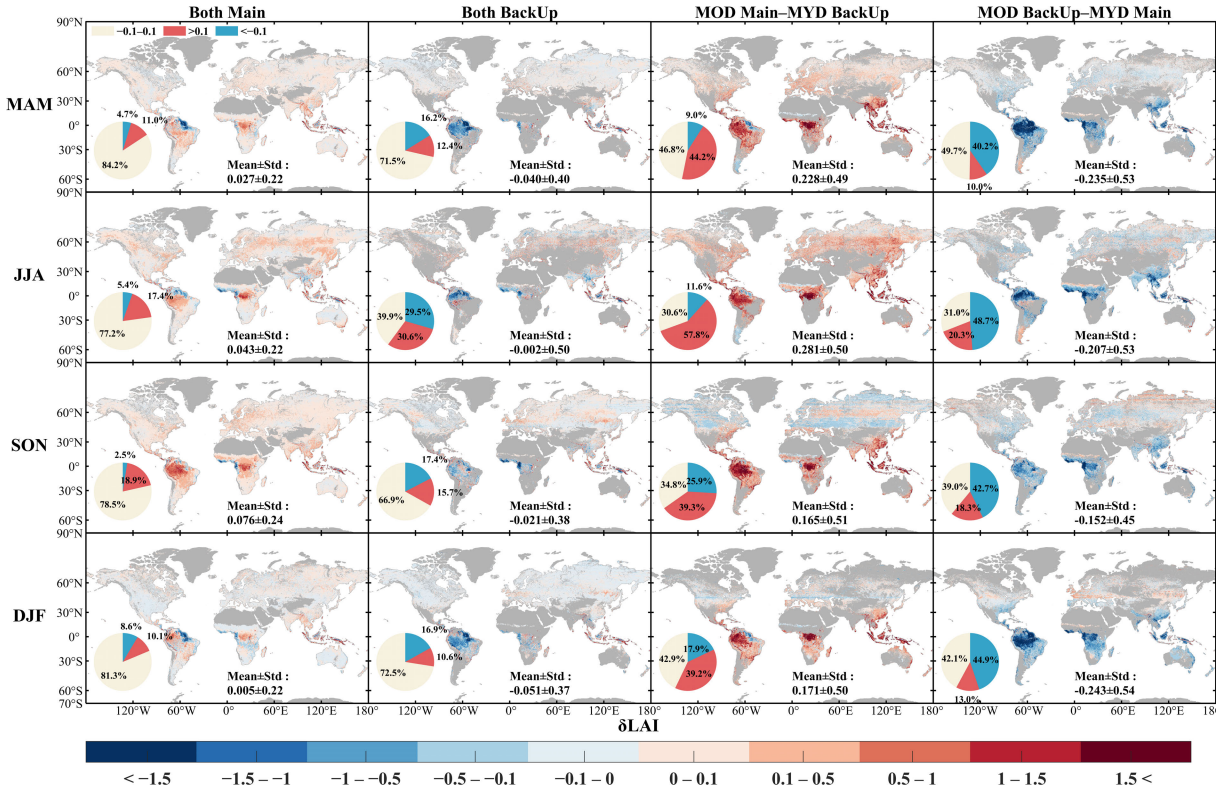

Fig. 5. Global distribution of LAI differences (MOD15A2H–MYD1512H) for different combinations of Terra and Aqua algorithms for the period 2003–2021. Results are from seasonal means and multiyear means of each composite difference.

showed LAI differences within ±0.5, and less than 1% of the retrievals exceeded LAI differences above ±1.5, indicating that the LAI distributions of the main algorithms for the Terra and Aqua sensors were consistent, with no systematic bias observed. When the algorithms were different, the percentage of retrievals with differences within ±0.5 decreased to less than 85%. Conversely, the percentage of pixels with differences exceeding ±1.5 increased and surpassed 2% across all

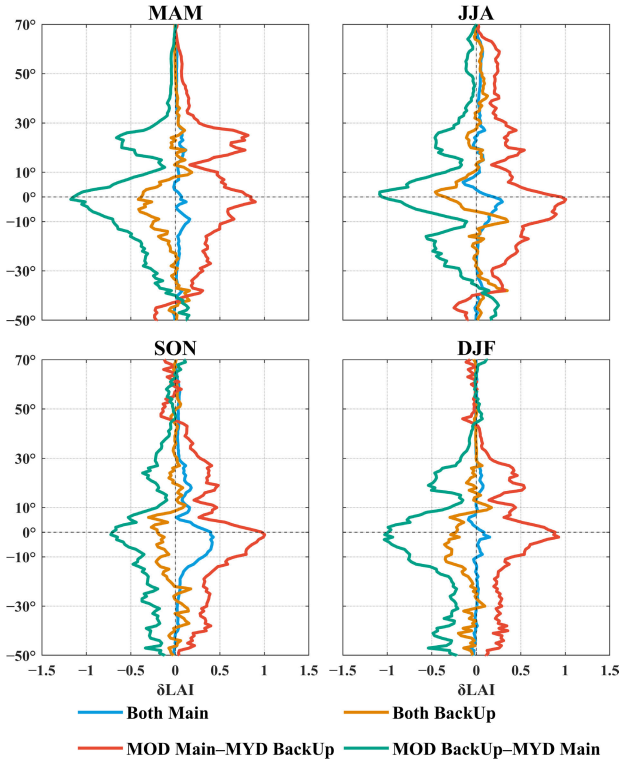

Fig. 6. Distribution of latitudinal mean differences for different algorithm LAI of MOD15A2H and MYD15A2H. The latitude interval is 1°.

four seasons. Notably, a portion of the pixels with larger differences originated from the tropical forest region (see Fig. 5).

Fig. 7 shows the frequency histograms of the LAI differences between two sensors. The LAI was more consistent with smaller mean differences and standard deviations when the algorithms were consistent. Conversely, inconsistent algorithms led to larger differences. The EBF biome type showed the greatest difference between the backup and main algorithms, with four-season difference means of 0.892, 0.884, 1.027, and 0.827 for the "MOD Main–MYD BackUp" and −1.106, −0.760, −0.596, and −1.046 for the "MOD BackUp–MYD Main," while 0.128, 0.224, 0.485, and 0.097 for "Both Main." When the algorithms were the same, the center of the difference curve was closer to 0, while the center line of the "MOD Main–MYD BackUp" was shifted to the right and the center line of the "MOD BackUp–MYD Main" was shifted to the left. Overall, the backup algorithm underestimates the LAI of the main algorithm, and this underestimation is most pronounced in the EBF biome type.

C. Spatiotemporal Correlation of Adjacent Years

We calculated the correlation of pixel pairs between two adjacent years for different algorithmic change scenarios to assess the internal consistency of the MODIS product (see Fig. 8). Fig. 8(a) shows that the correlation between the "Both Main" LAI pixel pairs is high at different latitudes, seasons, and vegetation types, in the range of [0.6, 0.9]. The correlation was noticeably lower when both years used backup algorithms or when the algorithm path was changed, within the range of [0.2, 0.6]. The R-values of the other three algorithm scenarios were more consistent with the "Both Main" scenario between 30°N and 60°N during the MAM. For biome types, the correlation was higher for non-forested vegetation (B1–B4) than for forested vegetation types (B5–B8). Fig. 8(b) shows the R-values after averaging over all seasons and latitudinal bands for each biome type. "Both Main" shows the highest correlation, while the correlation decreases for the remaining three algorithm scenarios. In addition, non-forested biomes (B1–B4) have higher correlations, and the biome type with the lowest correlation is B5 (EBF). Overall, the main and backup algorithms show noticeable inconsistencies. The correlation decreases when both years were backup algorithms or when the algorithm path changes. This indicates that the main algorithm exhibits higher stability, robustness, and responsiveness to natural vegetation variability.

By comparing the LAI bias of pixel pairs between two adjacent years, we can evaluate the impact of internal inconsistencies on short-term vegetation change monitoring. Fig. 8(c) shows that when the algorithm remained the same in two adjacent years, the LAI change exhibited relative stability, with a bias in the range of [−0.05, 0.05]. However, when there was a change in the algorithm, the magnitude of LAI changes increased. In the "Main to BackUp" scenario, LAI generally decreases, with a bias in the range of [−0.5, 0.1]. Conversely, in the "BackUp to Main" scenario, LAI generally increases, with a bias in the range of [−0.1, 1]. After averaging over all seasons and latitudinal bands for each biome type, we observed that a constant algorithm resulted in a small bias, whereas a varying algorithm led to a large bias [see Fig. 8(d)]. In addition, the exhibited similar magnitudes but with opposite positive and negative values. This difference was most pronounced in the B5 biome type, where the bias for "Both Main" and "Both BackUp" was nearly zero, while the absolute value of the bias for "Main to BackUp" and "BackUp to Main" exceeded 1 (−1.14 versus 1.16).

D. Impact of Inconsistency on 20-Year LAI Trends

The multiyear average GSA LAI from 2002 to 2021 indicates that in 99.25% of the vegetation pixels in the northern hemisphere, the Mixed LAI was lower than or approximately equal to the Main LAI [see Fig. 9(a)]. Among these, approximately 31.09% of the Mixed LAI had smaller values compared to the Main LAI. To quantify the effect of internal inconsistency on the stability of the LAI time series, we compared the CV of the main algorithm LAI and the Mixed LAI over a 20-year period [see Fig. 9(b)]. The results showed that the CV of Mixed LAI was greater than or approximately equal to that of Main LAI for 99.86% of the pixels, with 52.55% of the regions being greater. Regions with unequal CV values and mean GSA LAI were mainly found in the high latitudes of the northern hemisphere and in the tropics, where there tended to be a noticeable proportion of backup algorithm LAI in the time series. Overall, the internal inconsistency of the MODIS LAI product resulted in differences in the absolute magnitude of LAI values and heightened the probability of abnormal temporal fluctuations.

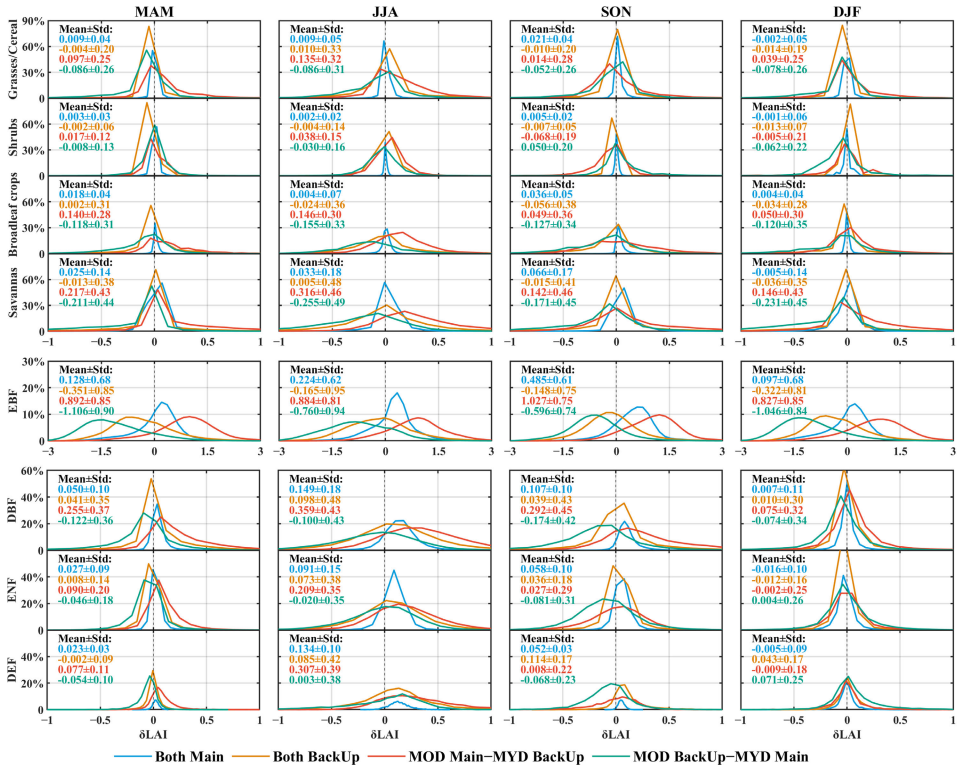

Fig. 7. Frequency histogram curves of LAI differences for different algorithm paths. These curves were generated from the data in Statistical Fig. 5, and the analysis only included pixels where the biome type did not change over 19 years. The bin size is set to 70.

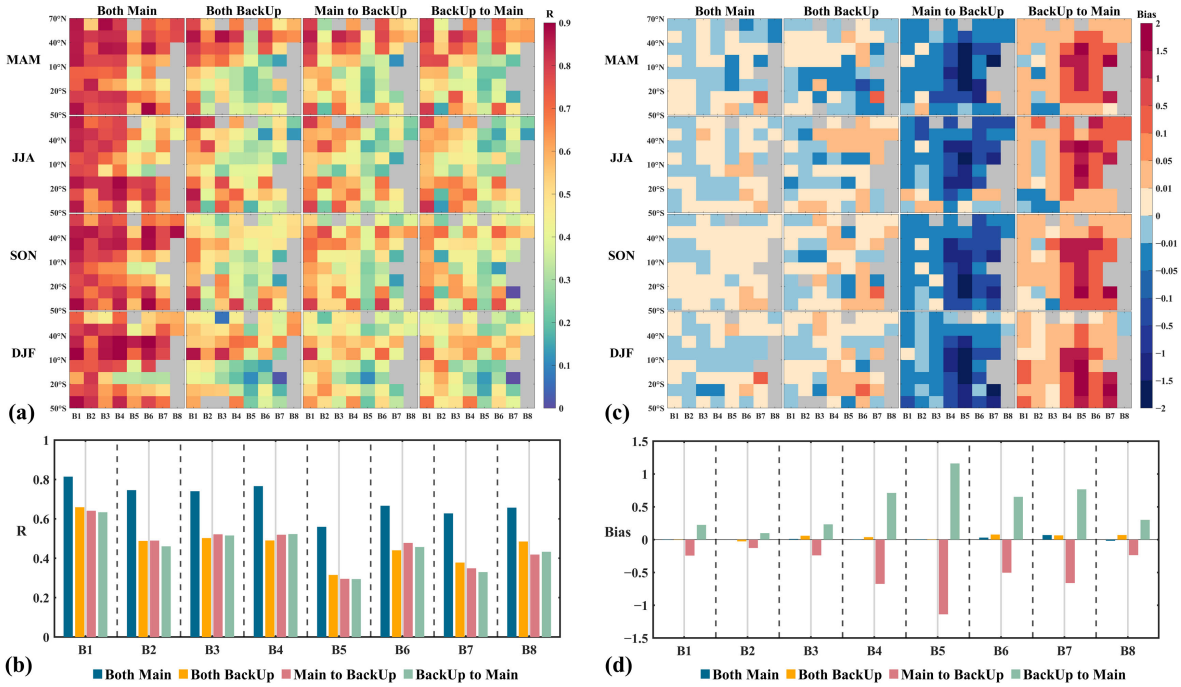

Fig. 8. (a) Heat map of R between pixel pairs for two adjacent years. (b) Mean values of R for LAI pixel pairs for all latitudinal bands and seasons across eight biome types. (c) Heat map of Bias between pixel pairs for two adjacent years. (d) Mean values of Bias for LAI pixel pairs for all latitudinal bands and seasons across eight biome types. Obtained by averaging three sets of results for 2003–2004, 2010–2011, and 2020–2021. Each grid cell represents all pixels of a particular biome type within the 15° latitude band. Only pixels with no change in vegetation type between adjacent years were used as analyzed pixels. Gray cells indicate a lack of vegetation pixels or fewer than 50 valid pixels.

Fig. 10 displays the spatial distribution of the trend test from 2002 to 2021, indicating that intra-product inconsistency has a minimal impact on the LAI trend test results. Without the MK test, approximately 82.04% of the vegetation area exhibited nearly equal annual changes between Main LAI and Mixed LAI, with larger differences concentrated in the

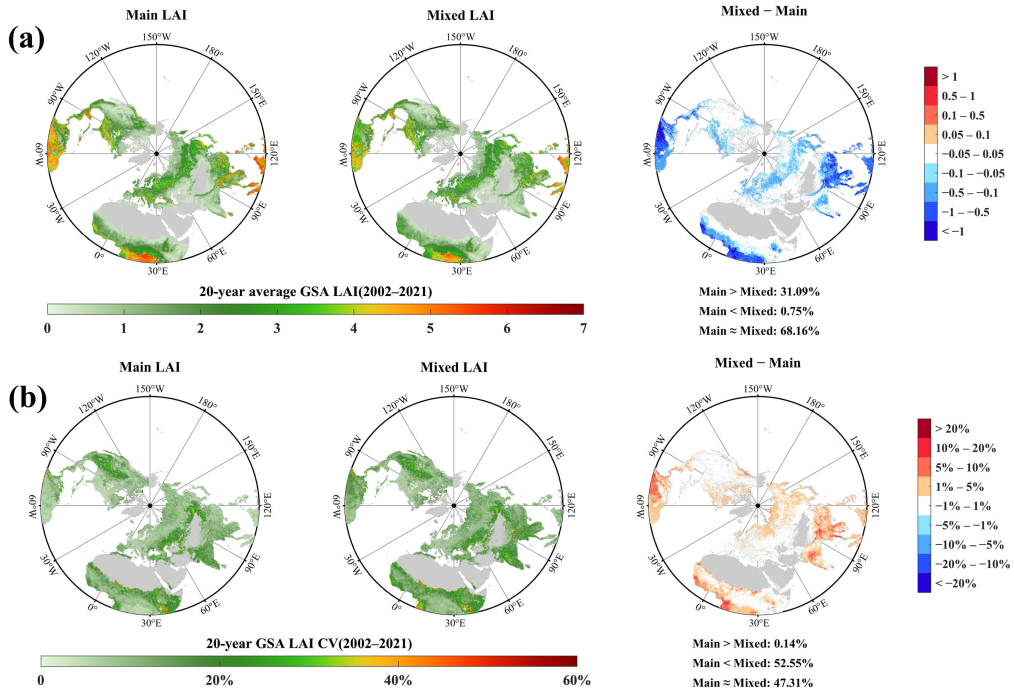

Fig. 9. Spatial distribution of GSA LAI in the northern hemisphere and their differences under different algorithm control methods. (a) Multiyear mean of GSA LAI for 2002–2021. (b) CV of GSA LAI time series for 2002–2021. The white areas on the surface are considered to be roughly equal when the differences are small.

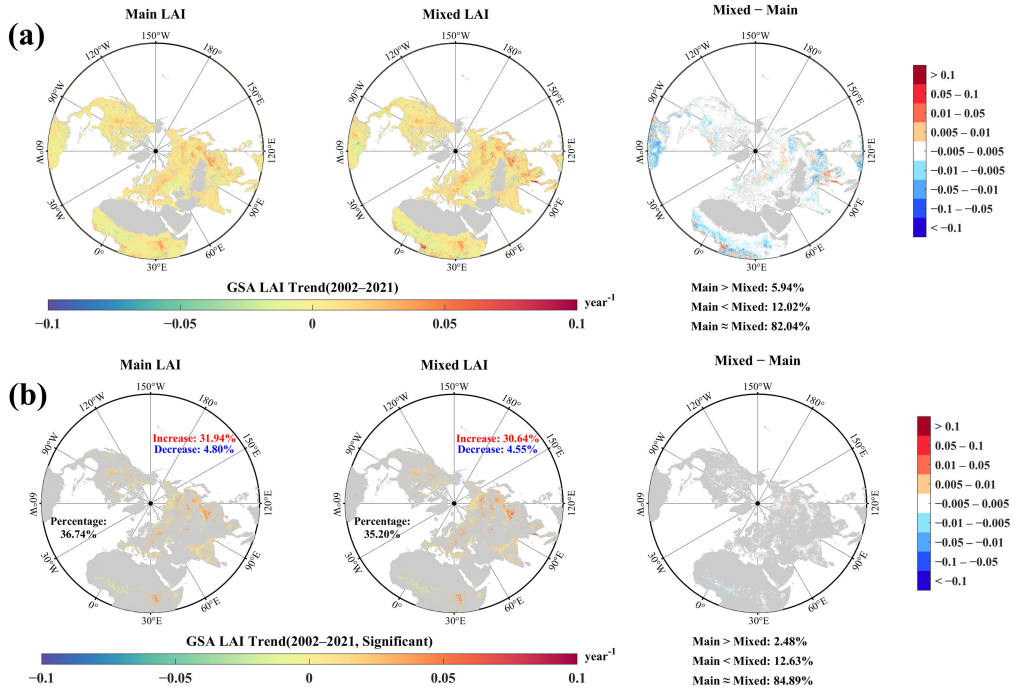

Fig. 10. Spatial distribution of GSA LAI trends and their differences under different algorithm control methods. (a) Trend estimates were based on Sen's slopes. (b) Trend estimates that passes the MK significance test ($p < 0.1$). The white areas on the surface are considered to be roughly equal when the differences are small.

tropics and high latitudes [see Fig. 10(a)]. The areas of the two algorithmic control methods that passed the trend test were very close in size ($p < 0.1$) and overlapped considerably [see Fig. 10(b)]. Among these regions, approximately 31.94% of pixels exhibited a significant increase in Main LAI, while 30.64% showed a significant increase in Mixed LAI. These increases were primarily concentrated in Asian regions, including China and India. Additionally, regions with a significant decrease accounted for 4.80% in Main LAI and 4.55% in Mixed LAI.

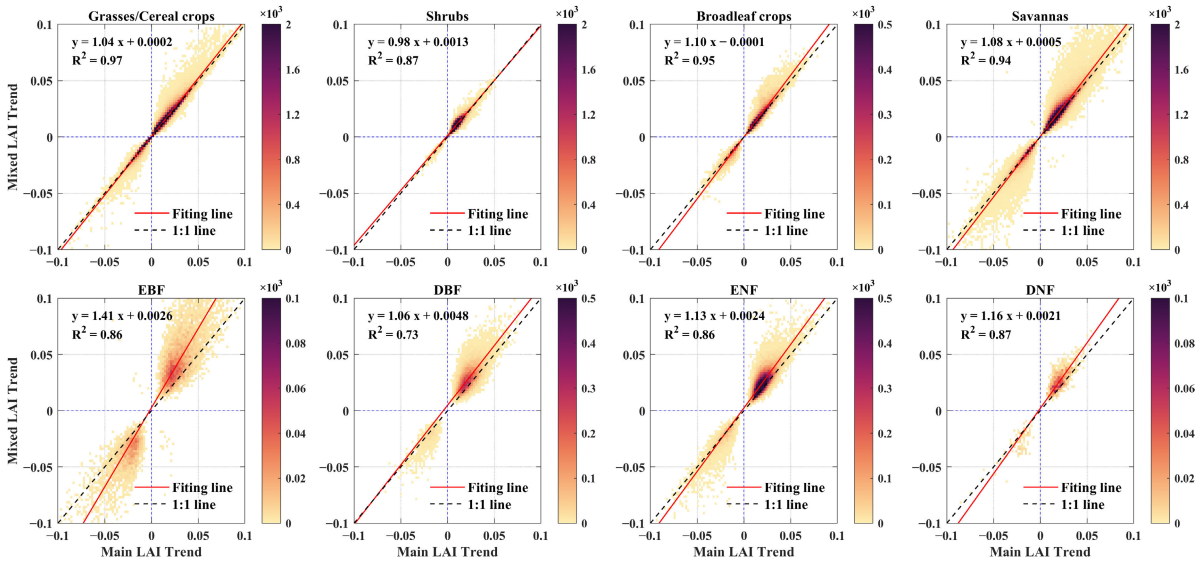

Fig. 11. Trend scatter density distribution of Main LAI and Mixed LAI. Only data that passed the trend test were counted. Only pixels with no change in land cover between 2002 and 2021 were used as analyzed pixels.

Fig. 11 shows the scatter density plots of Main LAI and Mixed LAI trends. The results showed that the trends of Main LAI and Mixed LAI were very consistent. The coefficients of determination (R^2) exceed 0.7 for all vegetation types, with grasses/cereal crops, broadleaf crops, and shrubs exhibiting the highest R^2 values (>0.94). Conversely, the lowest R^2 value was observed in the DBF biome type, with an R^2 of 0.73. Additionally, the trend consistency of the non-forested biome was higher than that of the forested biome, exhibiting a higher R^2 value, and the fit line is closer to the 1:1 line. The scatter points were predominantly distributed in the first quadrant, indicating a significant increasing trend for both Main LAI and Mixed LAI. However, a small number of scatter points in the second and fourth quadrants suggest an opposite trend for the shrub and EBF biome types. Fig. 12 illustrates the trend percentage plots for the different biome types under the two algorithmic control methods. The results indicate comparable trends between Main LAI and Mixed LAI for different biome types, with a difference of less than 3% in the percentages of significant increase and decrease. Main LAI shows a slightly higher percentage of significant increase compared to Mixed LAI in all vegetation types, except for B8 (DNF).

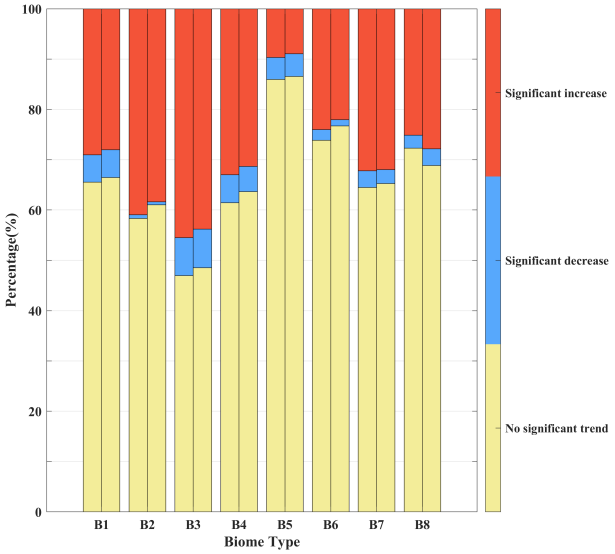

Fig. 12. Percentage of trends in Main LAI (left bars) and Mixed LAI (right bars) by biome type. The trend was categorized as no significant trend if it did not pass the significance test or passed the significance test but the absolute value of the change was less than 0.001 and as a significant increase (decrease) if it passed the significance test and the absolute value of the change was greater than 0.001. Only pixels with no change in land cover between 2002 and 2021 were used as analyzed pixels.

V. Discussion

A. Causes of Internal Inconsistencies

The "optimal" inversion algorithms for LAI products often cannot be implemented when inputting reflectance data with high uncertainty. This is due to suboptimal atmospheric corrections and poor observing conditions, such as cloud contamination, large angle observations, and snow/ice cover. As a result, "compromise" algorithms with poor precision, accuracy, and stability are used instead [19], [20], [26], [28], [29], [30], [31]. The first step in the MODIS LAI algorithm is to run the main algorithm. If the vegetation density is too high, the reflectance may become saturated. This saturation reduces the main algorithm's sensitivity to changes in canopy attributes, which may result in less accurate MODIS LAI seasonal variations [46]. In addition, when the sun-observation zenith angle is too large, the accuracy of the radiative transfer model will decrease. It also exacerbates the field-of-view effect of multiangle observations (where the observed range is larger than the true range), and the interaction of the radiative signal with the atmosphere is enhanced, leading to the failure of the main algorithms. When the atmospheric correction is unsatisfactory or there is ice/snow cover on the surface, the BRF may have large uncertainties, resulting in a decrease in the accuracy of the LAI/FPAR retrieval [47]. Additionally, MODIS LAI products use a biome map as

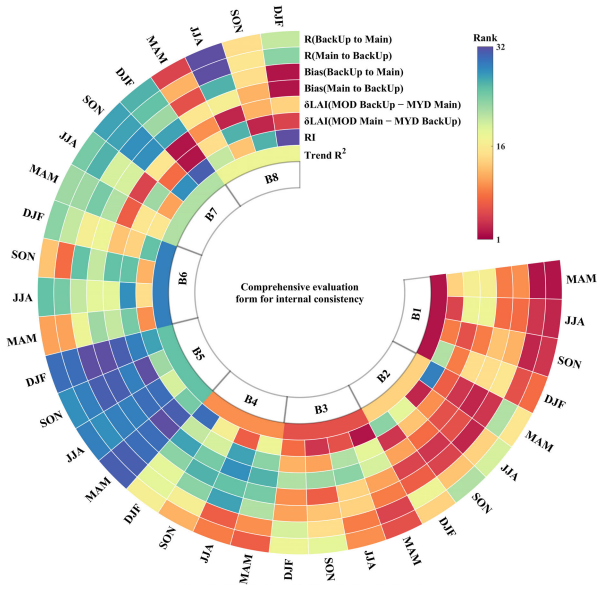

Fig. 13. Internal consistency of the eight biome types is comprehensively ranked based on the above results. A smaller rank indicates higher consistency or quality according to this index. Where Trend R^2 represents the trend consistency of Main LAI and Mixed LAI (growing season only); RI represents the proportion of main algorithm retrievals in 2021; δLAI indicates the difference in retrievals by different algorithms for Terra and Aqua, while R and Bias represent the correlation and bias of pixels in adjacent years.

a priori knowledge to minimize the unknowns of the "ill-posed" inverse problem [19], which can also lead to failure of the main algorithm when inaccurate biome classification maps are input [25]. Therefore, the primary reason for internal inconsistencies in the downstream LAI product is the variation in quality of the input upstream product.

Secondly, the "compromise" algorithms of existing LAI products have some limitations. In the MODIS LAI product, the backup algorithm is derived from the fitting correlation between the main algorithm LAI and its corresponding NDVI. This approach overcomes issues such as sensitivity to atmospheric conditions and background settings that arise when fitting LAI using a single band [48], [49]. However, in tropical and subtropical regions at low latitudes, NDVI is not effective in characterizing surface vegetation due to the saturation effect of NDVI [50]. This may explain the pronounced differences between the main and backup algorithms observed in the tropics in our study. For middle and high latitudes, the reflectance in the red and near-infrared bands increases noticeably when the surface is covered with snow and ice. This causes the NDVI to become close to 0 [51] and the backup algorithm will then provide LAI and FPAR retrieval results also close to 0 [35]. Finally, LAI is spatially heterogeneous, its relationship with NDVI is influenced by the phenological stage and is typically nonlinear [52]. Therefore, there are limitations in using empirical fitting methods to obtain the LAI-NDVI relationship.

B. Comprehensive Ranking of Internal Consistency of LAI Products

Fig. 13 summarizes the internal consistency rankings of products from different vegetation types and seasons. This section provides a summary comparison of the relevant indicators in the results. In this context, higher rankings indicate higher levels of internal consistency or product quality. Overall, we found that products with higher overall quality (RI) tended to perform better on other metrics. In terms of vegetation types, we found that the simpler vegetation showed better internal consistency. Specifically, internal consistency was noticeably higher for grasses/cereal crops (B1), shrubs (B2), and broadleaf crops (B3). The savannas (B4), DBF (B6), ENF (B7), and DNF (B8) had comparable internal consistency, but it was worse compared to grasses/cereal crops (B1), shrubs (B2), and broadleaf crops (B3). EBF (B5) had the lowest internal consistency and this biome type is predominantly found in tropical regions. Additionally, we observed that the internal consistency of the products varied with the seasons, with DNF (B8) being the most affected and EBF (B5) being the most stable. This is because reflectance product quality tends to correlate with the seasons. In winter, in mid to high-latitude regions, it is affected by snow and ice cover, resulting in very high surface reflectance. During cloudy and rainy seasons, it is affected by cloud cover and aerosols, resulting in higher reflectance uncertainty.

C. Potential Impact of Internal Inconsistency on LAI Applications

The LAI products have been widely utilized in various fields, including seasonal and interannual vegetation monitoring [53], regional phenological studies [54], [55], assessment and prediction of drought trends [56], [57], as well as the analysis of global greening trends [58], [59], [60]. Our study identifies internal inconsistencies in LAI products. This inconsistency is mainly reflected in the fact that the backup algorithm retrieval results tend to underestimate the main algorithm retrieval results. When performing short-term vegetation change estimation, algorithmic changes can lead to an overestimation of the magnitude of LAI change or even an incorrect determination of the greening and browning of vegetation [see Fig. 8(d)]. For trend analysis of long time series, the internal inconsistency of the product increases the volatility of the time-series data, but the effect on the results of the trend test is very small (see Fig. 10). This may be because the backup algorithm is built based on the empirical relationship between the main algorithm LAI and the corresponding NDVI for a specific vegetation type, thus maximizing the consistency between the backup algorithm LAI and the main algorithm LAI, and the differences that exist are systematic.

However, for studies that are more concerned with absolute values of LAI, such as surface system modeling, the internal inconsistency of the product may introduce greater uncertainty. Accurate LAI is a key biophysical parameter for modeling gross primary productivity (GPP) and evapotranspiration (ET), and is also critical for modeling the terrestrial carbon cycle [61]. Existing studies have shown that uncertainty in LAI products can lead to uncertainty in GPP and ET simulated by ecosystem models [62]. Inaccurate LAI may introduce considerable uncertainty into MODIS GPP estimates based on

light use efficiency models [63], and the problems of overestimation, underestimation, and discontinuity of MODIS LAI products over time limit their global application in modeling forest ecosystems' carbon cycle [63], [64], [65], [66].

D. Methods to Eliminate Product Internal Inconsistency

Eliminating internal inconsistencies in MODIS LAI products is crucial for their effective utilization. There are several possible solutions to explore. First, the original surface reflectance product could be reconstructed, thus removing the internal inconsistencies in the observations due to observation geometry and thick cloud cover [67]. Mismatches between biomes and specific LUTs can result in failure of the main algorithm or incorrect LAI values. Therefore, improvements can be made to the land cover classification algorithm and the auxiliary datasets used to obtain more accurate biome cover maps and reduce the proportion of backup algorithms [19], [68]. In addition, each vegetation index (VI) has its strengths and limitations, so it may be more appropriate to base the LAI–VI relationship on actual ground conditions or vegetation types. For example, it may be more appropriate to choose a VI with better resistance to saturation in densely forested areas, or to use a combination of multiple VI [50].

Surface reflectance is susceptible to influences from clouds, aerosols, and poor solar sensor geometry [69]. As a result, multiday compositing of daily products is often required. The MODIS LAI product utilizes a maximum fraction of photosynthetically active radiation (Max-FPAR) composite algorithm, which selects the best observations from an 8-day composite, thereby reducing potential reflectance errors [47]. However, inconsistencies in observation quality can lead to differences in time intervals (1–15 days) and algorithm paths between neighboring composites, which can impact the temporal smoothness of MODIS LAI products [70]. Therefore, employing more advanced multiday synthesis methods presents another effective approach to address internal inconsistencies in remote sensing products. For example, compared to the Max-FPAR composite method, the prior knowledge time-series composite algorithm (PKA) combines a linear kernel-driven (LKD) model with prior temporal knowledge, effectively improving the accuracy and temporal stability of LAI products [70].

Finally, existing remote sensing products can be reprocessed and reanalyzed to eliminate internal inconsistencies. An effective solution is to utilize the spatiotemporal correlation and quality information of the single product itself to reduce the noise level in the LAI time series. For example, the high-quality LAI product (HiQ-LAI) is generated by combining raw high-quality observations and spatiotemporal correlations from the MODIS C6.1 LAI product, which offers higher stability and reliability [71], [72]. Another approach is to integrate high-quality inversion results from multiple sensors to improve the overall quality of the product. For example, the sensor-independent (SI) LAI/FPAR CDR fuses high-quality LAI/FPAR retrievals from each of the Terra-MODIS/Aqua-MODIS/VIIRS sensors and applies spatiotemporal tensor (ST-Tensor) complete model to extrapolate the high-quality retrievals to other regions, resulting in a more stable, accurate, and internally consistent LAI product [73].

VI. Conclusion

Although many LAI validation studies have been conducted, the potential uncertainties and impacts of internal inconsistencies remain unknown because these efforts only use spatiotemporal invariant metrics to assess the products' overall quality. However, internally inconsistent LAI products can increase uncertainty in studies such as land surface process modeling, global primary productivity, water cycle, and carbon cycle analysis. Therefore, there is a pressing need for a new perspective and methodology to qualitatively and quantitatively evaluate the level of internal consistency of LAI products. In this study, the MODIS C6.1 LAI product was used as an example to comprehensively assess the consistency of different algorithmic retrieval results within the product. This assessment was based on multiproduct cross-validation and the spatiotemporal correlation of the product itself. The results show that there are certain inconsistencies in the MODIS LAI product, which are mainly reflected in the underestimation of the backup algorithm LAI compared to the main algorithm LAI. This underestimation is more severe in regions with dense tropical vegetation. Additionally, we found that the internal inconsistency of the products has a minimal effect on long time-series trend analysis. However, when making short-term vegetation change estimates, changes in the algorithm paths can lead to incorrect estimates of the magnitude and direction of change.

Under poor observational conditions, the best inversion algorithms of many remote sensing products often fail, so backup algorithms with poorer performance have to be used. This situation leads to widespread internal inconsistencies in the products. In order to eliminate these internal inconsistencies, several directions can be explored: improving the quality of the input data, using better backup algorithm, improving multiday composite algorithms, and reprocessing existing products. In summary, our results provide a new perspective on validating and evaluating global LAI products, which can help construct a more comprehensive evaluation system and ensure the rational application and improvement of these products. Additionally, we recommend that users refer to the data quality layers when using LAI products to select the appropriate data. If spatiotemporally continuous LAI data is not needed, it is recommended to only use the main algorithm retrieval. Otherwise, we recommend utilizing post-processed datasets with higher internal consistency, such as HiQ-LAI and SI LAI.

Acknowledgment

The authors appreciate valuable comments by anonymous reviewers on all versions of this article.

References

[1] N. R. Council, *Climate Data Records From Environmental Satellites: Interim Report*. Washington, DC, USA: National Academies Press, 2004.

[2] *Systematic Observation Requirements for Satellite-Based Data Products for Climate-2011 Update*, GCOS, WMO, Geneva, Switzerland, 2011.

[3] J. M. Chen, P. M. Rich, S. T. Gower, J. M. Norman, and S. Plummer, "Leaf area index of boreal forests: Theory, techniques, and measurements," *J. Geophys. Res., Atmos.*, vol. 102, no. D24, pp. 29429–29443, Dec. 1997.

[4] J. M. Chen and T. A. Black, "Defining leaf area index for non-flat leaves," *Plant, Cell Environ.*, vol. 15, no. 4, pp. 421–429, May 1992.

[5] R. B. Myneni et al., "Global products of vegetation leaf area and fraction absorbed PAR from year one of MODIS data," *Remote Sens. Environ.*, vol. 83, nos. 1–2, pp. 214–231, Nov. 2002.

[6] P. J. Sellers et al., "Modeling the exchanges of energy, water, and carbon between continents and the atmosphere," *Science*, vol. 275, no. 5299, pp. 502–509, Jan. 1997.

[7] J. M. Chen et al., "Vegetation structural change since 1981 significantly enhanced the terrestrial carbon sink," *Nature Commun.*, vol. 10, no. 1, p. 4259, Sep. 2019.

[8] S. Piao et al., "Characteristics, drivers and feedbacks of global greening," *Nature Rev. Earth Environ.*, vol. 1, no. 1, pp. 14–27, Dec. 2019.

[9] P. Sellers and D. Schimel, "Remote sensing of the land biosphere and biogeochemistry in the EOS era: Science priorities, methods and implementation—EOS land biosphere and biogeochemical cycles panels," *Global Planet. Change*, vol. 7, no. 4, pp. 279–297, Jun. 1993.

[10] S. T. Gower, C. J. Kucharik, and J. M. Norman, "Direct and indirect estimation of leaf area index, fAPAR, and net primary production of terrestrial ecosystems," *Remote Sens. Environ.*, vol. 70, no. 1, pp. 29–51, Oct. 1999.

[11] S. Burrows, S. Gower, and M. Clayton, "Application of geostatistics to characterize leaf area index (LAI) from flux tower to landscape scales using a cyclic sampling design," *Ecosystems*, vol. 5, pp. 667–679, Nov. 2002.

[12] Y. Knyazikhin, J. V. Martonchik, R. B. Myneni, D. J. Diner, and S. W. Running, "Synergistic algorithm for estimating vegetation canopy leaf area index and fraction of absorbed photosynthetically active radiation from MODIS and MISR data," *J. Geophys. Res., Atmos.*, vol. 103, no. D24, pp. 32257–32275, Dec. 1998.

[13] J. T. Morisette et al., "Validation of global moderate-resolution LAI products: A framework proposed within the CEOS land product validation subgroup," *IEEE Trans. Geosci. Remote Sens.*, vol. 44, no. 7, pp. 1804–1817, Jul. 2006.

[14] C. Justice, A. Belward, J. Morisette, P. Lewis, J. Privette, and F. Baret, "Developments in the 'validation' of satellite sensor products for the study of the land surface," *Int. J. Remote Sens.*, vol. 21, no. 17, pp. 3383–3390, Jan. 2000.

[15] P. B. Alton, "The sensitivity of models of gross primary productivity to meteorological and leaf area forcing: A comparison between a Penman–Monteith ecophysiological approach and the MODIS light-use efficiency algorithm," *Agricult. Forest Meteorol.*, vols. 218–219, pp. 11–24, Mar. 2016.

[16] S. Garrigues et al., "Validation and intercomparison of global Leaf Area Index products derived from remote sensing data," *J. Geophys. Res., Biogeosci.*, vol. 113, no. G2, Jun. 2008, doi: 10.1029/2007JG000635.

[17] D. Raymaekers et al., "SPOT-VEGETATION GEOV1 biophysical parameters in semi-arid Agro-ecosystems," *Int. J. Remote Sens.*, vol. 35, no. 7, pp. 2534–2547, Apr. 2014.

[18] F. Camacho, J. Cernicharo, R. Lacaze, F. Baret, and M. Weiss, "GEOV1: LAI, FAPAR essential climate variables and FCOVER global time series capitalizing over existing products. Part 2: Validation and intercomparison with reference products," *Remote Sens. Environ.*, vol. 137, pp. 310–329, Oct. 2013.

[19] K. Yan et al., "Evaluation of MODIS LAI/FPAR product collection 6. Part 1: Consistency and improvements," *Remote Sens.*, vol. 8, no. 5, p. 359, Apr. 2016.

[20] K. Yan et al., "Evaluation of MODIS LAI/FPAR product collection 6. Part 2: Validation and intercomparison," *Remote Sens.*, vol. 8, no. 6, p. 460, May 2016.

[21] H. Fang, Y. Wang, Y. Zhang, and S. Li, "Long-term variation of global GEOV2 and MODIS leaf area index (LAI) and their uncertainties: An insight into the product stabilities," *J. Remote Sens.*, 2021, doi: 10.34133/2021/9842830.

[22] B. Xu et al., "Analysis of global LAI/FPAR products from VIIRS and MODIS sensors for spatio-temporal consistency and uncertainty from 2012–2016," *Forests*, vol. 9, no. 2, p. 73, Feb. 2018.

[23] C. Di Bella, R. Faivre, F. Ruget, and B. Seguin, "Using VEGETATION satellite data and the crop model STICS-prairie to estimate pasture production at the national level in France," *Phys. Chem. Earth, A/B/C*, vol. 30, nos. 1–3, pp. 3–9, Jan. 2005.

[24] G. Murray-Tortarolo et al., "Evaluation of land surface models in reproducing satellite-derived LAI over the high-latitude northern Hemisphere. Part I: Uncoupled DGVMs," *Remote Sens.*, vol. 5, no. 10, pp. 4819–4838, Oct. 2013.

[25] J. Pu et al., "Evaluation of the MODIS LAI/FPAR algorithm based on 3D-RTM simulations: A case study of grassland," *Remote Sens.*, vol. 12, no. 20, p. 3391, Oct. 2020.

[26] B. Fuster et al., "Quality assessment of PROBA-V LAI, fAPAR and fCOVER collection 300 m products of Copernicus global land service," *Remote Sens.*, vol. 12, no. 6, p. 1017, Mar. 2020.

[27] F. Baret, M. Weiss, and A. Verger, "ATBD for LAI, FAPAR and FCOVER from PROBA-V products at 300m resolution (Geov3)," *IMAGINES_RP2.1_ATBD-LAI300M*, vol. 300, 2016. [Online]. Available: http://www.fp7-imagines.eu/media/Documents/ImagineS_RP2.1_ATBD-LAI300m_I1.73.pdf

[28] F. J. García-Haro et al., "Derivation of global vegetation biophysical parameters from EUMETSAT polar system," *ISPRS J. Photogramm. Remote Sens.*, vol. 139, pp. 57–74, May 2018.

[29] A. Verger et al., "GEOV2: Improved smoothed and gap filled time series of LAI, FAPAR and FCover 1 km Copernicus global land products," *Int. J. Appl. Earth Observ. Geoinformation*, vol. 123, Sep. 2023, Art. no. 103479.

[30] H. Ma and S. Liang, "Development of the GLASS 250-m leaf area index product (version 6) from MODIS data using the bidirectional LSTM deep learning model," *Remote Sens. Environ.*, vol. 273, May 2022, Art. no. 112985.

[31] K. Yan et al., "Generating global products of LAI and FPAR from SNPP-VIIRS data: Theoretical background and implementation," *IEEE Trans. Geosci. Remote Sens.*, vol. 56, no. 4, pp. 2119–2137, Apr. 2018.

[32] K. Yan et al., "A bibliometric visualization review of the MODIS LAI/FPAR products from 1995 to 2020," *J. Remote Sens.*, 2021, doi: 10.34133/2021/7410921.

[33] P. Myneni, MODIS Collection 6.1 (C6.1) LAI/FPAR Product User's Guide, 2020.

[34] D. Sulla-Menashe, and M. A. Friedl, "User guide to collection 6 MODIS land cover (MCD12Q1 and MCD12C1) product," *Usgs: Reston, Va, Usa*, vol. 1, p. 18, 2018.

[35] W. Yang et al., "Analysis of leaf area index products from combination of MODIS Terra and Aqua data," *Remote Sens. Environ.*, vol. 104, no. 3, pp. 297–312, Oct. 2006.

[36] W. R. Tobler, "A computer movie simulating urban growth in the Detroit region," *Econ. Geography*, vol. 46, p. 234, Jun. 1970.

[37] M. H. Kashani and Y. Dinpashoh, "Evaluation of efficiency of different estimation methods for missing climatological data," *Stochastic Environ. Res. Risk Assessment*, vol. 26, no. 1, pp. 59–71, Jan. 2012.

[38] S. Peng et al., "Asymmetric effects of daytime and night-time warming on northern Hemisphere vegetation," *Nature*, vol. 501, no. 7465, pp. 88–92, Sep. 2013.

[39] S. Piao, P. Friedlingstein, P. Ciais, L. Zhou, and A. Chen, "Effect of climate and CO_2 changes on the greening of the northern Hemisphere over the past two decades," *Geophys. Res. Lett.*, vol. 33, no. 23, 2006, doi: 10.1029/2006GL028205.

[40] C. E. Brown, "Coefficient of variation," in *Applied Multivariate Statistics in Geohydrology and Related Sciences*, C. E. Brown, Ed., Berlin, Germany: Springer, 1998, pp. 155–157.

[41] H. Abdi, "Coefficient of variation," *Encyclopedia Res. Des.*, vol. 1, no. 5, pp. 169–171, 2010.

[42] *World Meteorological Organization Guide to Climatological Practices*, World Meteorological Organization, Geneva, Switzerland, 2018.

[43] M. G. Kendall, "Rank correlation methods," Griffin, Oxford, U.K., 1948.

[44] H. B. Mann, "Nonparametric tests against trend," *Econometrica*, vol. 13, no. 3, p. 245, Jul. 1945.

[45] P. K. Sen, "Estimates of the regression coefficient based on Kendall's tau," *J. Amer. Stat. Assoc.*, vol. 63, no. 324, p. 1379, Dec. 1968.

[46] J. Heiskanen et al., "Seasonal variation in MODIS LAI for a boreal forest area in Finland," *Remote Sens. Environ.*, vol. 126, pp. 104–115, Nov. 2012.

[47] Y. Knyazikhin. (1999). *MODIS Leaf Area Index (LAI) and Fraction of Photosynthetically Active Radiation Absorbed by Vegetation (FPAR) Product (MOD15) Algorithm Theoretical Basis Document*. [Online]. Available: http://eospso.gsfc.nasa.gov/atbd/modistables.html

[48] R. Houborg and E. Boegh, "Mapping leaf chlorophyll and leaf area index using inverse and forward canopy reflectance modeling and SPOT reflectance data," *Remote Sens. Environ.*, vol. 112, no. 1, pp. 186–202, Jan. 2008.

[49] H. Kobayashi, N. Delbart, R. Suzuki, and K. Kushida, "A satellite-based method for monitoring seasonality in the overstory leaf area index of Siberian larch forest," *J. Geophys. Res., Biogeosci.*, vol. 115, no. G1, 2010, doi: 10.1029/2009JG000939.

[50] S. Gao et al., "Evaluating the saturation effect of vegetation indices in forests using 3D radiative transfer simulations and satellite observations," *Remote Sens. Environ.*, vol. 295, Sep. 2023, Art. no. 113665.

[51] D. K. Hall et al., "MODIS snow-cover products," *Remote Sens. Environ.*, vol. 83, nos. 1–2, pp. 181–194, 2002.

[52] N. Guindin-Garcia, A. A. Gitelson, T. J. Arkebauer, J. Shanahan, and A. Weiss, "An evaluation of MODIS 8- and 16-day composite products for monitoring maize green leaf area index," *Agricult. Forest Meteorol.*, vol. 161, pp. 15–25, Aug. 2012.

[53] X. Tang et al., "Monitoring the seasonal and interannual variation of the carbon sequestration in a temperate deciduous forest with MODIS time series data," *Forest Ecol. Manage.*, vol. 306, pp. 150–160, Oct. 2013.

[54] N. V. Shabanov, G. J. Marshall, W. G. Rees, S. A. Bartalev, O. V. Tutubalina, and E. I. Golubeva, "Climate-driven phenological changes in the Russian Arctic derived from MODIS LAI time series 2000–2019," *Environ. Res. Lett.*, vol. 16, no. 8, Aug. 2021, Art. no. 084009.

[55] Y. Song, J. Wang, Q. Yu, and J. Huang, "Using MODIS LAI data to monitor spatio-temporal changes of winter wheat phenology in response to climate warming," *Remote Sens.*, vol. 12, no. 5, p. 786, Mar. 2020.

[56] D. Liu, A. K. Mishra, Z. Yu, C. Yang, G. Konapala, and T. Vu, "Performance of SMAP, AMSR-E and LAI for weekly agricultural drought forecasting over continental United States," *J. Hydrol.*, vol. 553, pp. 88–104, Oct. 2017.

[57] A. G. Dhorde and N. R. Patel, "Spatio-temporal variation in terminal drought over Western India using dryness index derived from long-term MODIS data," *Ecolog. Informat.*, vol. 32, pp. 28–38, Mar. 2016.

[58] C. Chen et al., "China and India lead in greening of the world through land-use management," *Nature Sustainability*, vol. 2, no. 2, pp. 122–129, Feb. 2019.

[59] S. Piao et al., "Detection and attribution of vegetation greening trend in China over the last 30 years," *Global Change Biol.*, vol. 21, no. 4, pp. 1601–1609, Apr. 2015.

[60] Y. Zhang, C. Song, L. E. Band, G. Sun, and J. Li, "Reanalysis of global terrestrial vegetation trends from MODIS products: Browning or greening?" *Remote Sens. Environ.*, vol. 191, pp. 145–155, Mar. 2017.

[61] J. Kala et al., "Influence of leaf area index prescriptions on simulations of heat, moisture, and carbon fluxes," *J. Hydrometeorol.*, vol. 15, no. 1, pp. 489–503, Feb. 2014.

[62] Y. Liu et al., "Satellite-derived LAI products exhibit large discrepancies and can lead to substantial uncertainty in simulated carbon and water fluxes," *Remote Sens. Environ.*, vol. 206, pp. 174–188, Mar. 2018.

[63] F. A. Heinsch et al., "Evaluation of remote sensing based terrestrial productivity from MODIS using regional tower eddy flux network observations," *IEEE Trans. Geosci. Remote Sens.*, vol. 44, no. 7, pp. 1908–1925, Jul. 2006.

[64] X. Li et al., "Assimilating spatiotemporal MODIS LAI data with a particle filter algorithm for improving carbon cycle simulations for bamboo forest ecosystems," *Sci. Total Environ.*, vol. 694, Dec. 2019, Art. no. 133803.

[65] Z. Xiao, J. Wang, and Z. Wang, "Improvement of MODIS LAI product in China," *J. Remote Sens.*, vol. 12, no. 6, pp. 993–1000, 2008.

[66] Z. Xiao, S. Liang, J. Wang, B. Jiang, and X. Li, "Real-time retrieval of leaf area index from MODIS time series data," *Remote Sens. Environ.*, vol. 115, no. 1, pp. 97–106, Jan. 2011.

[67] X. Liang, Q. Liu, J. Wang et al., "Global 500 m seamless dataset (2000-2022) of land surface reflectance generated from MODIS products," *Earth Syst. Sci. Data Discuss.*, vol. 2023, pp. 1–40, Aug. 2023.

[68] M. A. Friedl et al., "MODIS collection 5 global land cover: Algorithm refinements and characterization of new datasets," *Remote Sens. Environ.*, vol. 114, no. 1, pp. 168–182, Jan. 2010.

[69] K. Yan et al., "Performance stability of the MODIS and VIIRS LAI algorithms inferred from analysis of long time series of products," *Remote Sens. Environ.*, vol. 260, Jul. 2021, Art. no. 112438.

[70] J. Pu et al., "Improving the MODIS LAI compositing using prior time-series information," *Remote Sens. Environ.*, vol. 287, Mar. 2023, Art. no. 113493.

[71] K. Yan, J. Wang, and R. Peng, "HiQ-LAI: A high-quality reprocessed MODIS LAI dataset with better spatio-temporal consistency from 2000 to 2022," *Earth Syst. Sci. Data Discuss.*, vol. 16, no. 3, pp. 1601–1622, 2024, doi: 10.1029/2009JG000939.

[72] J. Wang et al., "Improving the quality of MODIS LAI products by exploiting spatiotemporal correlation information," *IEEE Trans. Geosci. Remote Sens.*, vol. 61, 2023, Art. no. 4402319.

[73] J. Pu et al., "Sensor-independent LAI/FPAR CDR: Reconstructing a global sensor-independent climate data record of MODIS and VIIRS LAI/FPAR from 2000 to 2022," *Earth Syst. Sci. Data*, vol. 16, no. 1, pp. 15–34, Jan. 2024.

Xingjian Zhang received the B.S. degree from the Faculty of Land Resources Engineering, Kunming University of Science and Technology, Kunming, China, in 2022. He is currently pursuing the M.S. degree with the School of Information Engineering, China University of Geosciences, Beijing, China.

He is also a joint student of the Innovation Research Center of Satellite Application (IRCSA), Faculty of Geographical Science, Beijing Normal University. His research interests include vegetation remote sensing and particularly in the retrieval of vegetation parameter.

Kai Yan received the B.S. degree in mapping and surveying from Beijing University of Civil Engi-neering and Architecture, Beijing, China, in 2011, and the Ph.D. degree in geographic information system (GIS)/remote sensing (RS) from Beijing Normal University, Beijing, in 2018.

He was a Visiting Scholar with the Department of Earth and Environment, Boston University, Boston, MA, USA, from 2014 to 2016, and an Associate Professor with the School of Land Science and Techniques, China University of Geosciences, Beijing. He is currently an Associate Professor with the Faculty of Geographical Science, Beijing Normal University. He has been involved in the generation and assessment of official MODIS/VIIRS global leaf area index (LAI) and the fraction of photosynthetically active radiation absorbed by vegetation (FPAR) products. His research interests include land surface bidirectional reflectance distribution function (BRDF) modeling, RS big data and artificial intelligence, and LAI and FPAR mapping.

Jinxiu Liu received the M.Sc. degree in geographic information system (GIS) from Beijing Normal University, Beijing, China, in 2013, and the Ph.D. degree in geography from the University of Helsinki, Helsinki, Finland, in 2017.

She is currently an Associate Professor with the School of Information Engineering, China University of Geosciences, Beijing. Her research interests include time-series analysis with dense satellite data and vegetation remote sensing.

Kai Yang received the B.S. and M.S. degrees from the School of Land Science and Techniques, China University of Geosciences, Beijing, China, in 2021 and 2024, respectively.

His research interests include quantitative remote sensing of vegetation, RS big data, and artificial intelligence.

Jiabin Pu was born in Zhejiang, China. He received the M.E. degree from China University of Geosciences, Beijing, China, in 2022. He is currently pursuing the Ph.D. degree in geography with the Department of Earth and Environment, Boston University, Boston, MA, USA.

His research interests include remote sensing of vegetation.

Guangjian Yan (Senior Member, IEEE) received the Ph.D. degree from the Institute of Remote Sensing Applications, Chinese Academy of Sciences, Beijing, China, in 1999.

He is currently a Professor with the State Key Laboratory of Remote Sensing Science, Faculty of Geographical Science, Beijing Normal University, Beijing. He has published more than 300 articles. His research interests include multangular remote sensing, vegetation remote sensing, and radiation budget.

Janne Heiskanen received the M.Sc. degree in geography from the University of Turku, Turku, Finland, in 2003, and the Ph.D. degree in geography from the University of Helsinki, Helsinki, Finland, in 2008.

He is currently a University Researcher with the Department of Geosciences and Geography, University of Helsinki, and also with the Finnish Meteorological Institute, Helsinki. His research interests include remote sensing of vegetation parameters, land cover change, and water and carbon cycles.

Peng Zhu received the B.Eng. degree in remote sensing from Wuhan University, Wuhan, China, in 2011, the M.S. degree in geographic information science from the Chinese Academy of Sciences, Beijing, China, in 2014, and the Ph.D. degree in Earth and atmosphere science from Purdue University, West Lafayette, IN, USA, in 2018.

Prior to joining the University of Hong Kong (HKU), Hong Kong SAR, China, he was working at the University of California at San Diego, San Diego, CA, USA; Laboratoire des sciences du Climat et de l'environnement, Gif-sur-Yvette, France; and Sun Yat-sen University, Guangzhou, China. He is currently an Assistant Professor with the Department of Geography, HKU. His research interests include agroecosystem modeling, climate change impacts and adaptation, remote sensing, food-water-carbon nexus. Through integrating field observations, remote sensing, data-driven and process models, he aims to help stakeholders to better tackle climate risks, design effective climate adaptation strategies, and finally achieve agricultural sustainability.

Yuri Knyazikhin received the M.S. degree in applied mathematics from Tartu University, Tartu, Estonia, in 1978, and the Ph.D. degree in numerical analysis from the N. I. Muskhelishvili Institute of Computing Mathematics, Georgian Academy of Sciences, Tbilisi, Georgia, in 1985.

He was a Research Scientist with the Institute of Astrophysics and Atmospheric Physics, Tartu University, and also with the Computer Center of the Siberian Branch, Russian Academy of Sciences, Moscow, Russia, from 1978 to 1990. He worked with the University of Göttingen, Göttingen, Germany, from 1990 to 1996. He was an Alexander von Humboldt Fellow from 1992 to 1993. He is currently a Research Professor with the Department of Geography, Boston University, Boston, MA, USA. His work was published in the areas of numerical integral and differential equations, theory of radiative transfer in atmospheres and plant canopies, remote sensing of the atmosphere and plant canopies, ground-based radiation measurements, forest ecosystem dynamics, and modeling multifunctional forest management.

Ranga B. Myneni received the Ph.D. degree in biology from the University of Antwerp, Antwerp, Belgium, in 1985.

He is currently a Professor with Boston University, Boston, MA, USA. He is a Science Team Member of NASA Moderate Resolution Imaging Spectroradiometer (MODIS) and VIIRS Projects. He has authored over 330 scientific articles in peer-refereed journals and authored or co-authored over 250 scientific articles in peer-refereed journals. He has been a Highly Cited Researcher in geosciences and in environment and ecology for four years running since 2019. His research interests include remote sensing of vegetation and climate–vegetation interactions.